

High-performance Raman quantum memory with optimal control

Jinxian Guo^{1,2}, Xiaotian Feng¹, Peiyu Yang¹, Zhifei Yu¹, L. Q. Chen^{1*}, Chun-Hua Yuan¹ and Weiping Zhang^{2,3,*}

¹*School of Physics and Material Science, East China Normal University, Shanghai 200062, P. R. China*

²*Department of Physics and Astronomy, Shanghai Jiao Tong University, Shanghai 200240, China*

³*Collaborative Innovation Center of Extreme Optics, Shanxi University, Taiyuan, Shanxi 030006, China*

*Corresponding authors lqchen@phy.ecnu.edu.cn, wpzhang@phy.ecnu.edu.cn

Quantum memories with high efficiency and fidelity are essential for long-distance quantum communication and information processing. Techniques have been developed for quantum memories based on atomic ensembles. The atomic memories relying on the atom-light resonant interaction usually suffer from the limitations of narrow bandwidth. The far-off-resonant Raman process has been considered a potential candidate for use in atomic memories with large bandwidths and high speeds. However, to date, the low memory efficiency remains an unsolved bottleneck. Here, we demonstrate a high-performance atomic Raman memory in ^{87}Rb vapour with the development of an optimal control technique. A memory efficiency of 82.6% for 10-ns optical pulses is achieved and is the highest realized to date in atomic Raman memories. In particular, an unconditional fidelity of up to 98.0%, significantly exceeding the no-cloning limit, is obtained with the tomography reconstruction for a single-photon level coherent input. Our work marks an important advance of atomic Raman memory towards practical applications in quantum information processing.

Quantum memory is a necessary component for quantum communications and quantum computing. A practical quantum memory should be efficient, low-noise, broadband and as simple as possible to operate [1–6]. Using several approaches, including electromagnetically induced transparency (EIT), gradient echo memory (GEM), the off-resonant Faraday effect and far off-resonant Raman memory, optical memory has been demonstrated in cold atomic ensembles [2, 7], atomic vapours [8–11] and solids [12–14]. Yi-Hsin Chen et al. [15] reported a 96% memory efficiency for a coherent light pulse in a cold atomic ensemble using EIT. M. Hosseini et al. [16] used GEM to realize a 78% memory efficiency for weak coherent states with 98% fidelity. Polzik's group [10] demonstrated a quantum memory with a fidelity of 70% based on the off-resonant Faraday effect. These examples [10, 15, 16] successfully demonstrated the capability to store optical states with high efficiency and/or fidelity exceeding the classical limit [17–19] and sub-megahertz bandwidths. However, the bandwidth is important for the practical application of quantum memory [20]. Quantum sources with bandwidth at the GHz level have been used in long-distance quantum commu-

nication [21, 22] and quantum computers [23].

Unlike these protocols, far-off-resonant atomic Raman memory can store short-time pulses corresponding to high bandwidths and can operate at high speeds. In addition, the far-off-resonance characteristic makes the atomic Raman memory [8, 24, 25] robust against inhomogeneities in the ensemble and facilitates controlling the frequency of the output state. All of these properties indicate that atomic Raman memory has great potential in practical quantum information processing. The first experimental realization of an atomic Raman memory was demonstrated [24] in 2010. This achievement represented significant progress in the field of Raman memory, but some issues with low efficiency (<30%) and significant noise from the spontaneous four-wave mixing process persist. Recently, Raman memory using photonic polarized entanglement [25] in a cold atomic ensemble with a fidelity of $86.9 \pm 3.0\%$, but an efficiency of only $20.9 \pm 7.7\%$ was reported. An efficiency exceeding 50% and a fidelity exceeding 2/3 are necessary to store and retrieve an optical state within the no-cloning regime without post-selection [17–19, 26]. Therefore, previously, low efficiency appeared to exclude the broadband Raman memory as an unconditional quantum memory.

In this paper, we present an optimal control technique where the atomic vapour is performed a real-time optimal response on an input signal pulse. With a ^{87}Rb atomic vapour in paraffin-coated cell at $T=78.5^\circ\text{C}$, we achieve a Raman quantum memory on a 10-ns-long coherent input of photon number $n \approx 1$ with 82.6% memory efficiency and 98% unconditional fidelity.

I. EXPERIMENTAL SETUP

The experimental setup and atomic levels are depicted in Fig. 1. The ^{87}Rb atomic vapour in the paraffin-coated glass cell is the core component of the current Raman memory. The atomic cell is 10.0 cm long, has a diameter of 1.0 cm and is heated to 78.5°C . Our Raman memory starts with a large ensemble of atoms that were initially prepared in the $|m\rangle$ state by a 44- μs -long OP pulse. Then, the input signal pulse E_{in} is stored as atomic spin excitation S_W induced by the strong off-resonant write pulse (W) with the Rabi frequency $\Omega_W(t)$ and detuning Δ_W . After a certain delay τ , the atomic excitation can be retrieved into optical state E_R by the strong off-resonant read pulse (R) with the Rabi frequency $\Omega_R(t)$ and detun-

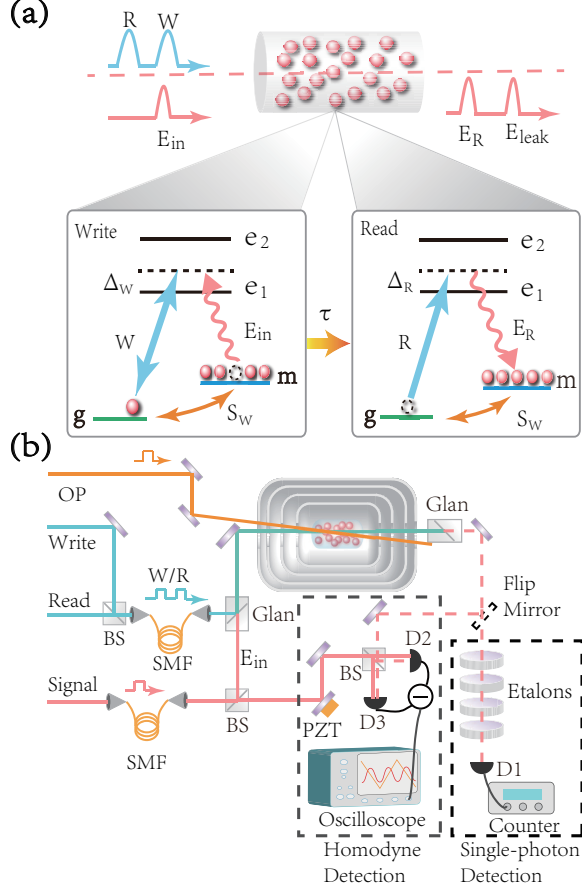


FIG. 1. **Raman memory.** (a) Schematic, atomic energy levels and frequencies of the optical fields. $|g, m\rangle$: hyperfine levels $|5^2S_{1/2}, F=1, 2\rangle$; $|e_1\rangle$ and $|e_2\rangle$: excited states $|5^2P_{1/2}, F=2\rangle$ and $|5^2P_{3/2}\rangle$. W : write field; E_{in} : input signal; E_{leak} : leaked signal; S_W : collective atomic spin wave; R : read field; E_R : retrieved signal. (b) Experimental setup. The polarizations of the weak signal beams, E_{in} and E_R , are perpendicular to the strong driving beams, W and R . The signals can be detected by a single-photon detector or by homodyne detection. OP: optical pumping laser; SMF: single-mode fibre; D1: single-photon detector; D2, D3: photo-detector; BS: beam splitter; PZT: piezoelectric transducer.

ing Δ_R . The waists of the laser beams (W , R and E_{in}) are all $600 \mu m$. The two strong driving beams, W and R , can be generated by the same or different lasers and are coupled into the same single-mode fiber. Their intensities and temporal shapes are controlled by acousto-optic modulators (AOMs). The input E_{in} signal comes from another laser phase-locked on the W laser. The temporal shape is controlled by a Pockels cell (Conoptics, model No. 360-80). The shortest pulse duration of the Pockels cell is 10 ns. The W and E_{in} fields are two-photon resonant and spatially overlapped after passing through a Glan polarizer with 94% spatial visibility in the atomic vapour. The output signals can be separated from the strong driving pulses by another Glan polarizer with an extinction ratio of 40 dB and are detected by a

homodyne detection or by a single-photon detector after passing through four etalons to filter the leaked driving photons at 115 dB with 33% transmission of the signal photons.

II. EXPERIMENTAL RESULTS

Efficiency

The Raman write process is a type of coherent absorption induced by a strong write pulse. As shown in Fig. 2(a), when the write pulse is switched off, owing to the far-off-resonant frequency, almost 100% of the E_{in} pulse passes through the atomic vapour. Below, we use the total energy of such an E_{in} pulse to normalize the write and retrieve efficiencies. When the write pulse is turned on, part of the energy of the E_{in} pulse is converted coherently as the atomic spin wave $S_W(z)$ near the two-photon resonance frequency. The rest of the E_{in} energy passes through the atoms as E_{leak} , as shown in Fig. 1(a). The full width at half maximum (FWHM) of the absorption spectrum is approximately 50 MHz, as shown in Fig. 2(a).

According to the theoretical analysis in Ref. [29], the spatial-distributed atomic spin wave in a far-off-resonant Raman write process is given by

$$S_W(z) = \int_0^{t_W} dt q(z, t) E_{in}(t) \quad (1)$$

where $q(z, t) = i \frac{\sqrt{d}}{\Delta_W} \Omega_W^*(t) e^{i \frac{dz + h(t, t_W)}{\Delta_W}} J_0(\frac{\sqrt{4h(t, t_W)} dz}{\Delta_W^2})$, t_W is the duration of the write process, d is the optical depth of atomic ensemble and $h(t, t_W) = \int_t^{t_W} |\Omega(t')|^2 dt'$. Eq. (1) is an iterative function that is determined by the matching between the temporal shapes of the input $E_{in}(t)$ and the write pulse $\Omega_W(t)$ [27–29]. Therefore, to achieve efficient conversion, it is crucial to perform real-time control on $\Omega_W(t)$ or $E_{in}(t)$ to make the atoms coherently absorb as much energy $E_{in}(t)$ as possible. The optimal control of $E_{in}(t)$ has been used to achieve efficient memory in an EIT-based process [15], where the shape of the input signal $E_{in}(t)$ was adjusted according to atomic memory system. Here, we prefer the dynamical control $\Omega_W(t)$ because a quantum memory system should have the ability to store and preserve quantum information of an input optical signal with an arbitrary pulse shape. To obtain the optimal $\Omega_W(t)$, denoted $\Omega_W^{opt}(t)$, we first use the iterative methods mentioned in Ref. [29] to calculate the optimal spin wave, corresponding to the minimum E_{leak} . Then, the optimal spin wave establishes a one to one correspondence between $E_{in}(t)$ and $\Omega_W^{opt}(t)$ via Eq. (1). Thus, for any given shape of $E_{in}(t)$, $\Omega_W^{opt}(t)$ can be obtained from Eq. (1) via the optimal spin wave. Moreover, the corresponding optimal efficiency η_W^{opt} depends on only the optical depth d and the total energy of the write pulse. Fig. 2(b) shows the theoretical efficiencies as the function of the energy of the strong driven

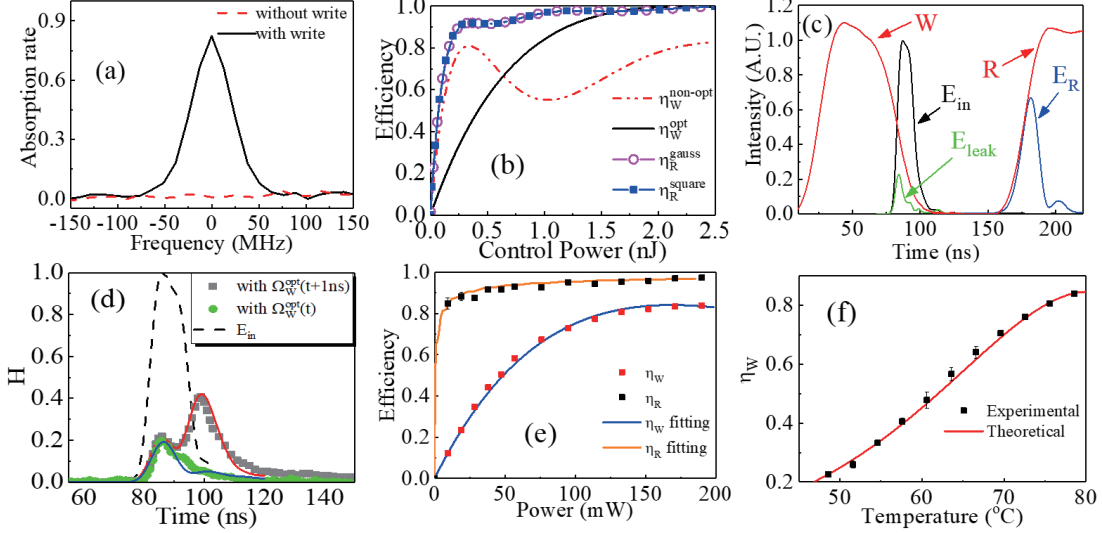


FIG. 2. Efficient Raman memory. (a) Absorption rate of the weak input-signal pulse as a function of the Raman detuning frequency. Δ_W is fixed at 3.0 GHz. (b) Theoretical efficiency as a function of the energy of the strong control pulse. The input optical pulse is a 10-ns near-square pulse. All optical fields detune 3.0 GHz from atomic transition and the optical depth $d = 1100$. In the write process, the efficiency is always much smaller than 1.0 when using a non-optimal write pulse (10-ns Gaussian shape), but it can approach 1.0 with the optimal write pulse when the write pulse is larger than 1.5 nJ. In the read process, the curves with Gaussian and square read pulses coincide with each other. The retrieval efficiency is waveform-independent and increases with the energy of the read pulse until approaching 1.0. (c) Temporal modes of the strong driving (red, W), input signal (black, E_{in}), leaked signal (green, E_{leak}) and output signal (blue, E_R) pulses. (d) Waveform of the leaked signal with the $\Omega_W^{opt}(t)$ (green dot) and $\Omega_W^{opt}(t+1ns)$ (gray square) write pulse. The lines are the corresponding theoretical fits. (e) Storage (η_W) and retrieval (η_R) efficiencies as functions of the power of the driving field with the optimized write pulse and the corresponding theoretical fitting. (f) The write efficiency as a function of the cell temperature.

pulses. Using a 10-ns near-square pulse as the input E_{in} , the write efficiency with $\Omega_W^{opt}(t)$ is approximately equal to 1 when the write energy is larger than 1.5 nJ, while the maximum write-in efficiency with a non-optimized $\Omega_W(t)$ (a 10-ns Gaussian-shaped $\Omega_W(t)$ is used in Fig. 2) is much smaller than one. In the read process (see Fig 1), the spin wave $S_W(z)$ is retrieved back to the optical field $E_R(t)$ by the read pulse $\Omega_R(t)$. Unlike η_W , the retrieval efficiency η_R is independent of the temporal waveform [29], and a read pulse with strong power but without temporal optimization is sufficient for $\eta_R \sim 1$. This can be seen in Fig. 2(b). η_R increases with the total energy of the read pulse, whether Gaussian or square-shaped until $\eta_R \sim 1$. Thus, with the above optimal control on $\Omega_W(t)$, the total efficiency of the Raman memory process is $\eta_T = \eta_W \times \eta_R \sim 1$ in principle.

Here, we experimentally demonstrate a break of the efficiency in Raman memory with dynamic control over the temporal shape of the write pulse. In the experiment, the given E_{in} pulse is mapped in a forward-retrieval configuration. We derive $\Omega_W^{opt}(t)$ using the iteration-based optimization strategy based on the given short $E_{in}(t)$ pulse and experimentally control the temporal profile of the write pulse by using an intensity modulator (here, an AOM). The temporal profile of the optimized write pulse is shown in Fig. 2(c). To show the magic improvement of optimization control, two write pulses are given,

the optimal $\Omega_W^{opt}(t)$ and an optimal write pulse delayed by 1.0 ns, $\Omega_W^{opt}(t+1ns)$. The corresponding leaked optical pulses and the theoretical fits are shown in Fig. 2(d). The leaked energy for the square curve is twice that for the dot curve. Through the optimal control, the leaked energy of the input signal is greatly reduced. The storage efficiency η_W , calculated by $(\bar{N}_{E_{in}} - \bar{N}_{E_{leak}}) / \bar{N}_{E_{in}}$, reaches $\sim 84\%$ when the atomic temperature T is 78.5°C and the power of the write pulse is 190 mW (Fig. 2(e)). The retrieval efficiency η_R , calculated by $\bar{N}_{E_R} / (\bar{N}_{E_{in}} - \bar{N}_{E_{leak}})$, can reach 98.5% when the read laser is 190 mW, with 3.0 GHz frequency detuning (Fig. 2 (e)). The total memory efficiency, $\eta_T = \eta_W \times \eta_R$, is 82.6% when the input signal pulse contains an average number of photons ranging from 0.4 to 10^4 ; thus, this Raman memory is a good linear absorber. The 82.6% memory efficiency is the best performance reported to date for Raman-based memory and far exceeds the no-cloning limit.

Fidelity

Fidelity is the ultimate performance criterion for quantum memory and reflects the maintenance of the quantum characteristics of the optical signal during the memory process. At the few-photon level, fidelity is readily degraded by excess noise and is mainly caused by the four-wave mixing (FWM) process [8] and spontaneous emission. Spontaneous noise comes from the spontaneous Raman scattering between the strong write pulse

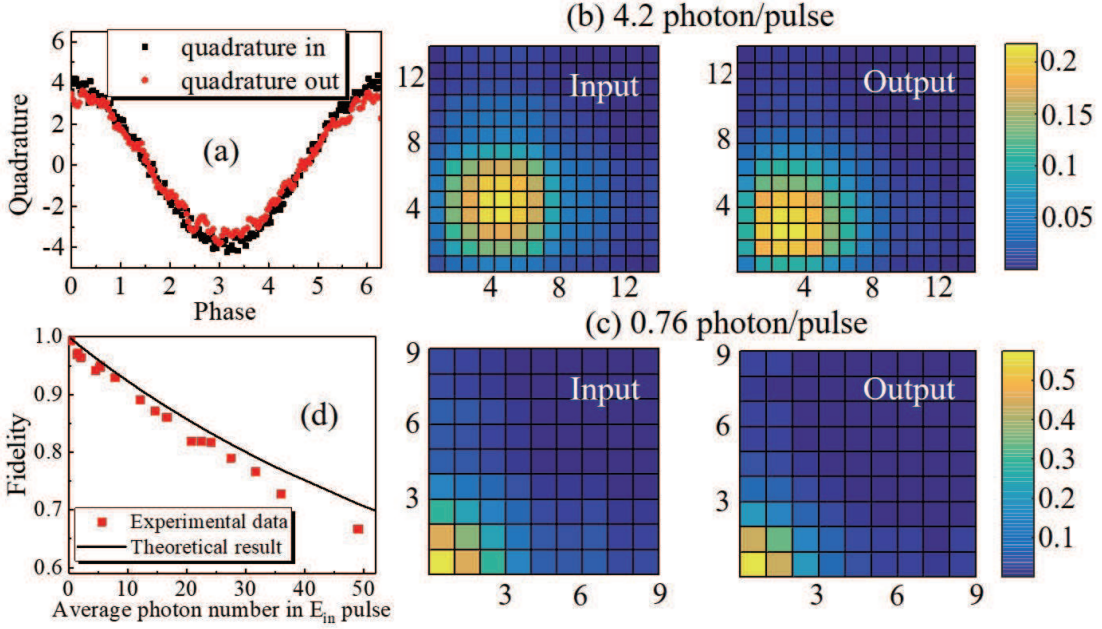


FIG. 3. **Fidelity of the Raman memory.** (a) Quadrature amplitudes of the input and output signal pulses at an average of 7.9 photons/pulse. The density matrices of the input and output signal pulses at 4.2 (b) and 0.76 (c) photons/pulse on average. (d) Fidelity as a function of the number of photons contained in the input signal pulse. The red squares show the experimental data, and the black line shows the theoretical result.

and the atoms populating the $|g\rangle$ state. Having fewer $|g\rangle$ atoms helps suppress the spontaneous excess noise. In our paraffin-coated cell, more than 98% of the atoms populate the $|m\rangle$ state. The spontaneous emission noise intensity is measured by determining the photon number using a single-photon detector when the E_{in} pulse is turned off. On average, the spontaneous noise is approximately 0.02 photons per memory process before the etalons for two strong driving pulses with a power of 190 mW at a detuning frequency of 3.0 GHz. The FWM excess noise is mainly attributed to anti-Stokes (AS_{FWM} , with same frequency of E_R) and Stokes (S_{FWM}) photons with the same intensity. We can deduce the proportion of AS_{FWM} in retrieved E_R pulse by measuring the intensity of S_{FWM} using single-photon detection. Our results show that the AS_{FWM} noise is less than 10% in E_R . Such low excess noise effectively guarantees the fidelity of the quantum memory process.

To achieve the fidelity performance of the current Raman quantum memory, we measure the fidelity using the equation $F = |Tr(\sqrt{\rho_{in}\rho_{out}}\sqrt{\rho_{in}})|^2$ [30], where ρ_{in} and ρ_{out} are the reconstructed density matrices of E_{in} and E_R , respectively. We record the quadrature amplitudes of the E_{in} and E_R signals using homodyne measurement, and we then reconstruct the density matrices by tomographic reconstruction [31]. The setup used for homodyne detection is shown in Fig. 1(b). To stabilize the phase difference between the E_{in} and E_R pulses and simplify the homodyne setup, the write and read pulses are generated by the same laser and are controlled using

one AOM. In the measurement, the two weak signals, E_{in} and E_R , are both short pulses. Matching the temporal modes of short pulses is difficult. Therefore, we use a strong continuous laser beam with the same frequency as the signal pulses E_{in} and E_R as the local oscillator for homodyne detection (the detailed strategy can be found in Refs. [31, 32]). We recorded 10^5 sets of quadrature amplitudes of the E_{in} and E_R pulses while varying the phase of the local oscillator between 0 and 2π by scanning the piezoelectric transducer, multiplying the quadrature amplitudes of each pulse by the pulse shapes of the corresponding signals, and finally, integrating the product over the signal pulse duration. The integrated quadrature amplitude as a function of the local oscillator phase is shown in Fig. 3(a), where the mean number of photons contained in the E_{in} pulse is 7.9. The phase of the retrieved E_R signal pulse closely follows that of the input E_{in} pulse.

The density matrix elements of the E_{in} and E_R pulses are obtained based on the quadrature-amplitude results using the maximum-likelihood reconstruction method [31, 33]. The results are plotted in Fig. 3(b,c), with the input pulses containing, on average, 4.2 and 0.76 photons, corresponding to unconditional fidelities of 0.915 and 0.98, respectively. The fidelities significantly exceed the no-cloning limit, indicating that the current Raman memory is a quantum-memory process and does not introduce significant excess noise during the memory process.

As mentioned above, the current Raman memory is

a good linear absorber and allows the storage and retrieval of coherent optical signals at the single-photon level for up to 10^4 photons with the same memory efficiency. Unlike the efficiency, the unconditional fidelity of the quantum memory of the coherent field is related to the average photon number contained in the input signal ($\bar{N}_{E_{in}}$) and efficiency (η_T) by $F = 1/[1 + \bar{N}_{E_{in}}(1 - \sqrt{\eta_T})^2]$ [19], which shows that if $\eta_T < 1$, the fidelity will rapidly decrease with $\bar{N}_{E_{in}}$ owing to the worse overlap between ρ_{in} and ρ_{out} . In Fig. 3(d), the fidelity is shown as a function of $\bar{N}_{E_{in}}$ with $\eta_T = 82.6\%$. The experimental F value is slightly smaller than the theoretical F value because of the excess noise in the experiment. F exceeds the no-cloning limit [34–36] at $\bar{N}_{E_{in}} \leq 49$ in the current Raman memory process.

Bandwidth and coherence time

Raman memory is a genuine broadband memory. The ability to store and retrieve broadband pulses was successfully demonstrated in Ref. [24], where a bandwidth larger than 1 GHz of the retrieved signal was obtained using a 300 ps and 4.8 nJ read pulse. In a practical Raman memory, the bandwidth is generated dynamically by the strong driving pulses. In Fig. 2(c), the E_{in} pulse has a FWHM of 10 ns and a bandwidth of 100 MHz. The FWHM of the E_R signal pulse is 13 ns, corresponding to a bandwidth of 77 MHz. The 77 MHz bandwidth of the single E_R signal in the current memory is dozens or hundreds of times larger than the values reported based on the EIT, Faraday and GEM approaches, thus demonstrating the broadband memory ability of the current quantum memory scheme.

The decoherence time, which is another essential criterion for good quantum memory, is measured to be approximately 1.1 μ s in the present atomic system and is mainly limited by the diffusion of the atoms [37]. The delay-bandwidth product at 50% memory efficiency, an appropriate figure of merit, is defined as the ratio of the memory time to the duration of the signal pulse and is 52 in this work.

In summary, we have demonstrated a high-performance broadband quantum optical memory via pulse-optimized Raman memory in free space. The 82.6% memory efficiency is the highest value obtained

to date for far-off-resonant Raman memory. The unconditional fidelity of 98% for an input pulse containing an average of approximately one photon significantly exceeds the classical limit. The 77 MHz bandwidth of the current memory is dozens or hundreds of times larger than the reported bandwidths for memories based on the EIT, Faraday and GEM approaches. The delay-bandwidth product at 50% memory efficiency is 52. These attractive properties demonstrate that the Raman memory is a high-performance broadband quantum memory. Additionally, our memory is implemented in an atomic vapour system that can be easily operated and could become the core of a scalable platform for quantum information processing, long-distance quantum communication and quantum computation.

Further improvement of the performance could be achieved by improving the experimental conditions. Higher efficiency could be achieved by increasing the atomic optical depth through increasing the atomic temperature (Fig. 2(e)), lengthening the cell, or obtaining better spatial-mode matching. The bandwidth could be improved to 1 GHz by using shorter and stronger driving pulses [24]. The decoherence time or the delay-bandwidth product at 50% memory efficiency is limited by atomic diffusion out of the laser beam in the current memory system. It could be increased to as high as 10^5 by using an anti-relaxation-coated cell [10] with the same diameter as the laser beams, for which the typical decoherence time is approximately several milliseconds.

Acknowledgements

This work was supported by the National Key Research and Development Program of China under grant number 2016YFA0302001, and by the National Natural Science Foundation of China (grant numbers 91536114, 11474095, and 11654005), and National Science Foundation of Shanghai (No. 17ZR1442800).

Competing financial interests

The authors declare no competing financial interests.

-
- [1] Fleischhauer, M. & Lukin, M. D. Dark-State polaritons in electromagnetically induced transparency. *Phys. Rev. Lett.* **84**, 5094 (2000).
 - [2] Liu, C., Dutton, Z., Behroozi, C. H., & Hau, L. V. Observation of coherent optical information storage in an atomic medium using halted light pulses. *Nature* **409**, 490 (2001).
 - [3] Phillips, D. F., Fleischhauer, A., Mair, A., Walsworth, R. L., & Lukin, M. D. Storage of light in atomic vapor. *Phys. Rev. Lett.* **86**, 783 (2001).
 - [4] Mair, A., Hager, J., Phillips, D. F., Walsworth, R. L., & Lukin, M. D. Phase coherence and control of stored photonic information. *Phys. Rev. A* **65**, 031802(R) (2002).
 - [5] Honda, K. *et al.* Storage and retrieval of a squeezed vacuum. *Phys. Rev. Lett.* **100**, 093601 (2008).
 - [6] Appel, J., Figueroa, E., Korystov, D., Lobino, M. & Lvovsky, A. I. Quantum memory for squeezed light. *Phys. Rev. Lett.* **100**, 093602 (2008).
 - [7] Zhao, R. *et al.* Long-lived quantum memory. *Nature Phys.* **5**, 100 (2008).
 - [8] Reim, K. F. *et al.* Single-Photon-Level quantum memory at room temperature. *Phys. Rev. Lett.* **107**, 053603 (2011).
 - [9] Hosseini, M., Sparkes, B. M., Campbell, G., Lam, P. K.,

- & Buchler, B. C. High efficiency coherent optical memory with warm rubidium vapour. *Nat. Commun.* **2**, 174 (2011).
- [10] Julsgaard, B., Sherson, J., Cirac, J. I., Fiurasek, J., & Polzik, E. S. Experimental demonstration of quantum memory for light. *Nature* **432**, 482-486 (2004).
- [11] van der Wal, C. H., *et. al* Atomic memory for correlated photon states. *Science* **301**, 196 (2003).
- [12] Longdell, J. J., Fraval, E., Sellars, M. J., & Manson, N. B. Stopped light with storage times greater than one second using electromagnetically induced transparency in a solid. *Phys. Rev. Lett.* **95**, 4 (2005).
- [13] Bigelow, M. S., Lepeshkin, N. N. & Boyd, R. W. Superluminal and slow light propagation in a room-temperature solid. *Science* **301**, 200 (2003).
- [14] Chaneliere, T., Ruggiero, J., Bonarota, M., Afzelius, M., & Gout, J-L L. Efficient light storage in a crystal using an atomic frequency comb. *New J. Phys.* **12**, 023025 (2010).
- [15] Chen, Y.-H. *et. al.* EIT-based photonic memory with near-unity storage efficiency. Preprint at <https://arxiv.org/abs/1605.08519> (2016).
- [16] Hosseini, M., Campbell, G., Sparkes, B. M., Lam, P. K., & Buchler, B. C. Unconditional room-temperature quantum memory. *Nature Phys.* **7**, 794 (2011).
- [17] Grosshans, F. & Grangier, P. Quantum cloning and teleportation criteria for continuous quantum variables. *Phys. Rev. A* **64**, 010301 (2001).
- [18] Hétet, G., Peng, A., Johnsson, M. T., Hope, J. J., & Lam, P. K. Characterization of electromagnetically-induced-transparency-based continuous-variable quantum memories. *Phys. Rev. A* **77**, 012323 (2008).
- [19] He, Q. Y., Reid, M. D., Giacobino, E., Cviklinski, J. & Drummond, P. D. Dynamical oscillator-cavity model for quantum memories. *Phys. Rev. A* **79**, 022310 (2009)
- [20] Simon, C., *et. al.* Quantum memories. *Eur. Phys. J. D* **58**, 1-22 (2010).
- [21] Halder, Matthäus, *et. al.* High coherence photon pair source for quantum communication. *New. J. Phys.* **10**, 023027 (2008).
- [22] Rakher, Matthew, T., *et. al.* Simultaneous wavelength translation and amplitude modulation of single photons from a quantum dot. *Phys. Rev. Lett.* **107**, 082602 (2011).
- [23] Lounis, Brahim & Orrit, Michel, Single-photon sources, *Rep. Prog. Phys.* **68**, 1129-1179 (2005).
- [24] Reim, K. F. *et. al.* Towards high-speed optical quantum memories. *Nature Photon.* **4**, 218 (2010).
- [25] Ding, D.-S. *et. al.* Raman quantum memory of photonic polarized entanglement. *Nature Photon.* **9**, 332-338 (2015).
- [26] Varnava, M., Browne, D. & Rudolph, T. Loss tolerance in one-way quantum computation via counterfactual error correction. *Phys. Rev. Lett.* **97**, 120501 (2006).
- [27] Nunn, J. *et. al.* Mapping broadband single-photon wave packets into an atomic memory. *Phys. Rev. A* **75**, 011401(R) (2007).
- [28] Wasilewski, Wojciech, & Raymer, M. G., Pairwise entanglement and readout of atomic-ensemble and optical wave-packet modes in traveling-wave Raman interactions. *Phys. Rev. A* **73**, 063816(2006).
- [29] Gorshkov, A. V., André, A., Lukin, M. D., & Sørensen, A. S., Photon storage in Λ -type optically dense atomic media. II. Free-space model. *Phys. Rev. A* **76**, 033805 (2007).
- [30] Nielsen, D. A. & Chuang, I. L. *Quantum Computation and Quantum Information* (Cambridge University Press, Cambridge, 2000).
- [31] Paris, M. & Řeháček, J. *Quantum State Estimation* (Springer Berlin Heidelberg, 2004).
- [32] Raymer, M. G., Cooper, J., Carmichael, H. J., Beck, M. & Smithey, D. T. Ultrafast measurement of optical-field statistics by dc-balanced homodyne detection *J. Opt. Soc. Am. B* **12**, 1801(1995).
- [33] Lvovsky, A. I. Iterative maximum-likelihood reconstruction in quantum homodyne tomography. *J. Opt. B: Quantum Semiclass. Opt.* **6**, S556-S559 (2004).
- [34] Hétet, G., Peng, A., Johnsson, M. T., Hope, J. J., & Lam, P. K., Characterization of electromagnetically-induced-transparency-based continuous-variable quantum memories. *Phys. Rev. A* **77**, 012323 (2008).
- [35] Grosshans, F. & Grangier, P. Quantum cloning and teleportation criteria for continuous quantum variables. *Phys. Rev. A* **64**, 010301 (2001).
- [36] Varnava, M., Browne, D. E., & Rudolph, T., Loss tolerance in one-way quantum computation via counterfactual error correction. *Phys. Rev. Lett.* **97**, 120501 (2006).
- [37] Camacho, R. M., Vudyssetu, P. K., & Howell, J. C. Four-wave-mixing stopped light in hot atomic rubidium vapour. *Nature Photon.* **3**, 103 (2009).